RESEARCH ARTICLE

# The potential failure of Monte Nuovo at Ischia Island (Southern Italy): numerical assessment of a likely induced tsunami and its effects on a densely inhabited area

**F. Zaniboni · G. Pagnoni · S. Tinti · M. Della Seta · P. Fredi · E. Marotta · G. Orsi**

**Abstract** Ischia is the emergent top of a large volcanic complex that rises more than 1,000 m above the sea floor, at the north-western end of the Gulf of Naples. Caldera resurgence in the central part of the island has resulted in the formation of differentially displaced blocks, among which Mt. Epomeo (787 m a.s.l.) is the most uplifted. Deformation and slope instability have been recognised as common features induced by a block resurgence mechanism that causes uplift and favours gravitational loading and flank failure. The Monte Nuovo block, a topographic high on the north-western flank of Mt. Epomeo, has recently been interpreted as a block affected by deep-seated gravitational slope deformation. This block may undergo a catastrophic failure in the case of renewal of magmatic activity. This paper investigates the potential failure of the Monte Nuovo block as a rockslide-debris avalanche, the consequent tsunami generation and wave propagation, and discusses the catastrophic effects of such an event. Mobilization-prone volume has been estimated at about $160 \cdot 10^6$ m$^3$ and would move from a maximum elevation of 400 m a.s.l. The landslide itself would sweep away a densely populated territory as large as 3.5 km$^2$. The highest waves generated by the tsunami, on which this paper is mainly focussed, would hit the northern and western shores of Ischia. However, the high coast would prevent inundation and limit devastation to beaches, harbours and surrounding areas. Most of the tsunami energy would head towards the north-east, hitting the Campania coast. Severe inundation would affect an area of up to 20 km$^2$ around the mouth of the Volturno river, including the urban area of Castel Volturno. In contrast, less energy would travel towards the south, and the Gulf of Naples would be perturbed by long persisting waves of limited damaging potential.

**Keywords** Numerical simulation · Landslide tsunami · Volcanic instability · Tsunami hazard

## Introduction

Volcanic islands are among the sources of the most catastrophic known tsunamis, which may be triggered by high magnitude eruptions and volcanic edifice collapse, as at Santorini, Greece, in the Late Bronze Age (see McCoy and Heiken 2000, and references therein) or at Krakatau, Indonesia, in 1883 (Francis 1985). To perform a complete tsunami hazard assessment in such areas, not only very rare large-volume collapses, but also smaller and more frequent events like lateral slope failures, have to be taken into account. Seismicity associated with magmatic or volcanic activity, as well as overloading from accumulation of newly erupted rocks, and overpressuring from dike intrusion, can generate gravitational instability, while steep slopes, a common feature on most volcanic islands, induce high velocity in rock slides, and hence increase their tsunamigenic potential. Tsunamis in volcanic areas account for ca. 6 % of the total recorded events (e.g. NGDC/WDS database; containing more than 2,400 entries). This percentage is probably an underestimate since some events, attributed to an unknown cause, we infer to be the result of unwitnessed submarine or subaerial volcanic landslides.

F. Zaniboni (✉) · G. Pagnoni · S. Tinti
Dipartimento di Fisica e Astronomia, Alma Mater
Studiorum—Università degli Studi di Bologna, viale Carlo Berti
Pichat 6/2, 40127 Bologna, Italy
e-mail: filippo.zaniboni@unibo.it

M. Della Seta · P. Fredi
Dipartimento di Scienze della Terra, Università degli Studi di Roma
"La Sapienza", Piazzale Aldo Moro 5, 00185 Rome, Italy

E. Marotta · G. Orsi
Istituto Nazionale di Geofisica e Vulcanologia, Sezione di Napoli
"Osservatorio Vesuviano", via Diocleziano 328, 80124 Naples, Italy

Numerical simulations of volcanic tsunamis include the Late Bronze Age Santorini volcano-tectonic collapse (Pareschi et al. 2006); the 1741 lateral collapse of Oshima-Oshima volcano, Japan (this tsunami, considered one of the most catastrophic events in the Japan Sea, caused more than 2,000 casualties; Satake and Kato 2001; Satake 2007); the 1883 Krakatau caldera collapse, Indonesia (the resulting tsunami killed about 36,000 people in the Sunda Straits; Nomanbhoy and Satake 1995; Choi et al. 2003); the 5 km³ lateral collapse of Ritter Island, Papua New Guinea, 1888 (the largest recorded event in historical times in the area; Ward and Day 2003); the 2002 retrogressive failure of 30-40·10⁶ m³ of material at Stromboli, Italy (Tinti et al. 2006; Chiocci et al. 2008); and the 2003 dome-collapse of Soufrière Hills at Montserrat, Lesser Antilles, 2003 (Pelinovsky et al. 2004). Numerical simulations have been used also to forecast the generation and propagation of tsunamis, such as the one that would be induced by a potential collapse of 150 to 500 km³ of Cumbre Vieja in the Canary Islands, which would affect the entire North Atlantic ocean (Ward and Day 2001; Abadie et al. 2012 and references therein).

The volcanic island of Ischia, located in the southern Tyrrhenian Sea (Italy), at the north-western end of the Gulf of Naples, has already been studied from this point of view. Bathymetric surveys have highlighted the existence of extended deposits south of the island, interpreted as the products of a single catastrophic event that occurred in historical times from the southern slopes of Mt. Epomeo, named the Ischia Debris Avalanche (IDA; Chiocci and de Alteriis 2006; de Alteriis et al. 2010). The IDA dynamics, its tsunamigenic potential and tsunami propagation in the Gulf of Naples and along the Campanian coasts have been computed elsewhere (Tinti et al. 2011).

Other submarine deposits, resulting from further minor collapses, have been found around the western and northern coasts of Ischia by de Alteriis and Violante (2009). These authors did not directly associate them with submarine or subaerial scars along the slopes of Mt. Epomeo, although they genetically related them to the dynamics of the Ischia volcanic system. Indeed, the dominant feature of the area is an ongoing block resurgence, begun at 33 ka (Orsi et al. 1991; de Vita et al. 2006) that has caused frequent mass failures, with failed mass occasionally reaching the sea and generating tsunamis.

Recent geological and geomorphological investigations on Mt. Epomeo (Della Seta et al. 2011) have confirmed that historical debris avalanches, debris flows, and "Deep-Seated Gravitational Slope Deformations" (DSGSD) occurred as a consequence of the Mt. Epomeo uplift. Some of the subaerial failure scars and deposits were correlated with parts of the offshore deposits found by de Alteriis and Violante (2009), thus demonstrating that such slope failures, in addition to having catastrophic effects in their source areas, have the potential to generate tsunamis and therefore to affect the

neighbouring and densely inhabited Campanian coast. Large-scale and relatively slow mass movements such as DSGSD, which generally have low probability to evolve into debris avalanches, can still in a worst-case scenario have catastrophic effects. Moreover, provided that structural and geological conditions favour failure, this probability increases in case of seismic shocks. In particular, in the case of renewal of resurgence in response to magmatic activity, the Monte Nuovo DSGSD block and some densely fractured portions of the western and northern high-angle slopes of Mt. Epomeo are potential source areas for destructive failures.

To assess effects of such a failure, we have carried out a study focussed on the possible rapid mobilization, as a rockslide-debris avalanche (sensu Glicken 1998), of the Monte Nuovo DSGSD block, hereafter called the Monte Nuovo Slide (MNS). According to our reconstruction, based on application of the numerical codes already used to study the IDA tsunami (Tinti et al. 2011), the MNS would be about 160·10⁶ m³ in volume with its head located at 400 m a.s.l. After characterising its geometry, we have computed its downslope motion and simulated the induced tsunami propagation and impact on Ischia and on the coast of the Campanian region, including the Gulf of Naples.

## Geological outlines and slope instability

The island of Ischia is the subaerial portion of a large volcanic complex (Orsi et al. 1999; Bruno et al. 2002) whose base lies more than 1,000 m b.s.l. at the north-western end of the Gulf of Naples. It is an active volcanic field within the Phlegraean Volcanic District, that also encompasses the island of Procida and the Phlegraean Fields caldera (Orsi et al. 2003; Fig. 1a).

The volcanic history of Ischia began prior to 150 ka (Vezzoli 1988) and continued, with centuries to millennia of quiescence, until the most recent eruption in AD 1302 (Buchner 1986). Ischia is one of the most impressive examples of a resurgent caldera in the world. It formed after a high-magnitude explosive eruption that produced the Mt. Epomeo Green Tuff (MEGT) complex sequence at c. 55 ka (Brown et al. 2008). Since the MEGT eruption, volcanism has been concentrated in three periods of activity from 55–33 ka, 28–18 ka, and <10 ka, with almost all the most recent vents located

Fig. 1 a Location of the study area and structural sketch map of the ▶ Neapolitan volcanic area. b Geological sketch map of Ischia (modified after Orsi et al. 2003; bathymetry after de Alteriis et al. 2005). c Morphostructural map of the western portion of Ischia, and distribution of the main gravitational landforms. d Monte Nuovo DSGSD and its corollary of minor mass movements with a radial pattern, detached from within the deformed mass. Diagnostic features, such as a significant counter-slope scarp (delimited by NE-SW, ENE-WSW and N-S trending major fault segments) and bulging of the slope foot of the deformed block, are shown in plain view and along a topographic profile. (Modified after Della Seta et al. 2011)
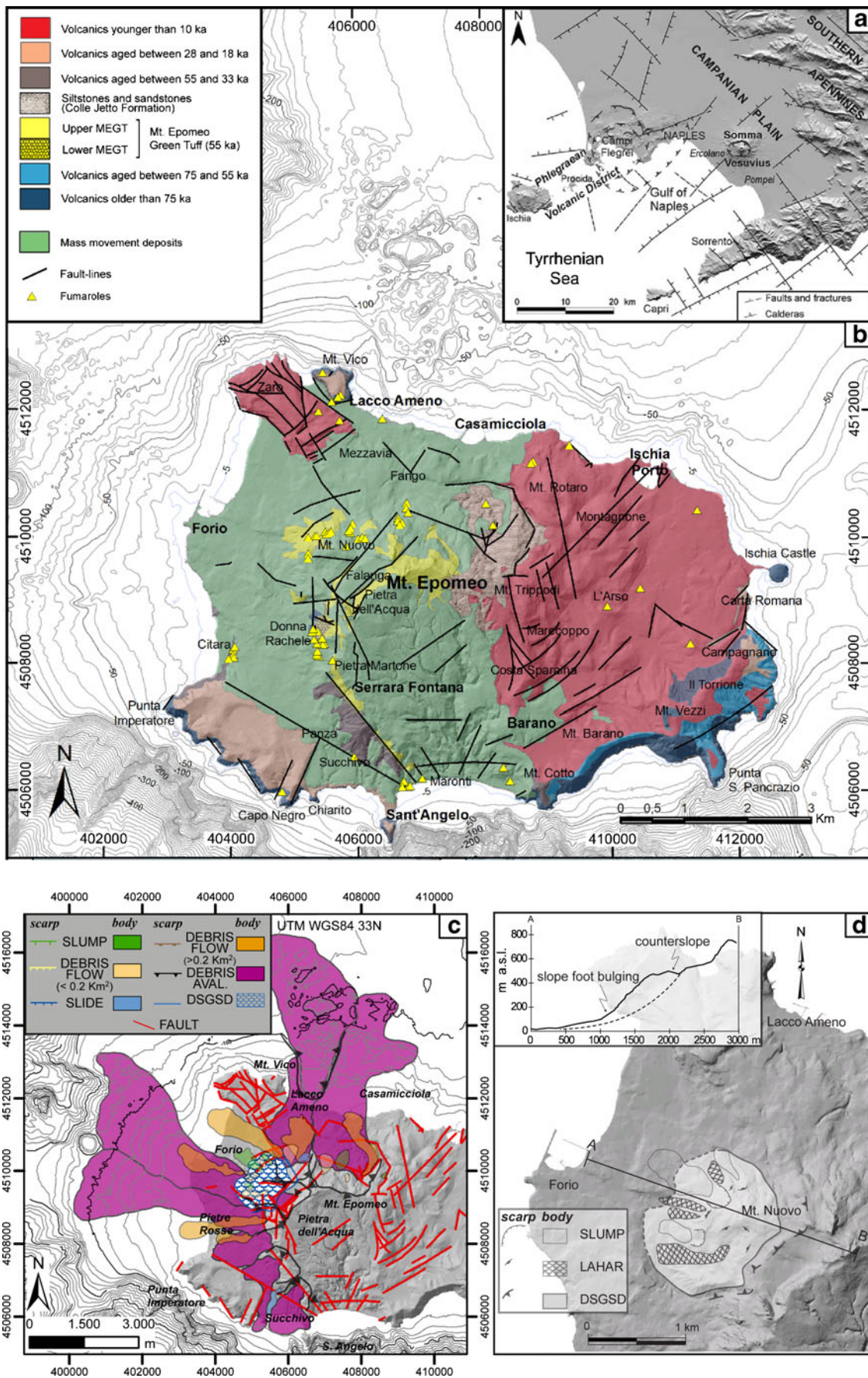
in the eastern sector of the island (Chiesa et al. 1987, 1988; Vezzoli 1988; Civetta et al. 1991, 1999; Orsi et al. 1991, 1996, 2003; de Vita et al. 2010). Caldera resurgence, begun around 33 ka, has generated a maximum net uplift of about 900 m of the Mt. Epomeo block (Orsi et al. 1991). The Mt. Epomeo resurgent block, delimited mainly by N40/50 W and N50/60E trending fault systems (Fig. 1b; Orsi et al. 1991; Acocella and Funiciello 1999; Acocella et al. 2004), has north-western flanks that are considerably steeper and shorter than the south-eastern ones, as a result of an asymmetrical uplift.

An intimate interplay exists between slope instability, volcanism, resurgence dynamics, hydrothermal system structure, fault generation, and seismicity at Ischia (Chiodini et al. 2004; de Vita et al. 2006). In particular, alternating constructive and destructive phases in the evolution of the island are testified to by the emplacement of volcanic rocks, epiclastic deposits and subordinate terrigenous sediments (Vezzoli 1988; Orsi et al. 1991, 2003; de Vita et al. 2006, 2010; Di Napoli et al. 2009, 2011).

Many historical chronicles of natural phenomena such as earthquakes, volcanic eruptions, ground deformation and slope instability events can be found for the Neapolitan area, including Ischia, because it has been inhabited by an organised society since the eighth century BC (Buchner 1986; Civetta et al. 1999; Orsi et al. 2003; Del Prete and Mele 2006; Della Seta et al. 2011). Della Seta et al. (2011) correlated depositional landforms to reported historical slope instability events, and have identified the products of several volcano-tectonically triggered mass movements occurring in the northern and western sectors of the island since 5.5 ka (Fig. 1c). Using a quantitative approach to the analysis of landforms (Ciotoli et al. 2003; Della Seta et al. 2005), the authors have concluded that phenomena such as debris avalanches, lahars and a DSGSD occurred during critical periods for mass movement generation that alternated with eruptive periods. After the last eruption in AD 1302, only minor mass movements triggered by earthquakes were activated between 1797 and 1883 along the north-facing slopes of the island (Fig. 1c).

Debris avalanches have affected the slopes of the Mt. Epomeo resurgent block. Della Seta et al. (2011) have highlighted that the structures that drove resurgence and fed volcanism also played an important role in both generating the major debris avalanches and defining the location and geometry of their detachment areas (Fig. 1c). Furthermore, some of the debris avalanches likely flowed into the sea, as suggested by the bathymetry of the northern and western offshore of the island (D'Argenio et al. 2004; de Alteriis and Violante 2009), travelling up to 6 km from the source areas.

Mt. Nuovo covers an area of about 1.6 km$^2$ at the north-western corner of the Mt. Epomeo block (Fig. 1d) and shows diagnostic features (Della Seta et al. 2011) of a DSGSD (e.g. Ter Stepanian 1966; Radbruch-Hall et al. 1977; Varnes et al. 1988; Agliardi et al. 2001). It is a displaced portion of the Mt. Epomeo block, presently affected by an estimated westward displacement rate of maximum 15 mm·year$^{-1}$, on the basis of precision levelling, GPS surveys, and DInSAR data (Manzo et al. 2006; Sepe et al. 2009).

## Numerical simulations

The numerical simulation of the MNS motion and of the consequent tsunami has been carried out using the codes UBO-BLOCK1 and UBO-TSUFD (Tinti et al. 1997; Tonini et al. 2011) developed by the Tsunami Research Team of the University of Bologna. The two codes have been applied separately: the motion of the sliding body, considering also a possible underwater path, has been computed through UBO-BLOCK1. Since the discretisation methods for the two codes are different (Lagrangian for UBO-BLOCK1 and Eulerian for UBO-TSUFD) an interpolation mapping has been applied to convert variables from the landslide computational grid (which follows the sliding rock body) to the tsunami mesh (which is fixed in space). The forcing due to the landslide and resulting from the UBO-BLOCK1 application has been used as input to the tsunami simulation software UBO-TSUFD, which is a finite-difference code that can calculate tsunami propagation over a given domain. Further details on the analytical procedures used are reported in Appendix A.

Landslide simulation

The landslide simulation code UBO-BLOCK1 requires specification of the sliding surface and the initial landslide geometry. In our computation the slide is discretized as a chain of blocks, and the sliding surface is assumed to be the surface along which all blocks move downslope. It therefore comprises the surface of rupture (the surface underlying the initial mass), the surface of separation (the part of the ground surface covered by the final deposit) and the intermediate part of the surface swept by the moving mass. The sliding surface is provided as a topographic surface on a regular mesh of points (Fig. 2) and has been chosen following the morphological and geological characteristics of the Monte Nuovo DSGSD (Della Seta et al. 2011). In our computation this surface does not change with time, since the slide is assumed not to be accompanied by erosion or deposition during its downslope movement. Deposition only takes place when the landslide mass comes to rest. This simplifying assumption is acceptable in light of the involved volume and the rockslide-debris avalanche mechanism hypothesized for the collapse of the Monte Nuovo block.

The slide geometry is inferred from the volume contained between the sliding surface and the actual topography-bathymetry of Ischia. The initial thickness of the MNS exceeded 300 m (Fig. 2) and its volume is about 0.16 km$^3$. Other input data needed by the code UBO-BLOCK1 are the

**Fig. 2** MNS and the topo-bathymetry at and around the island of Ischia. Thicknesses of the reconstructed initial body and of the computed final deposit are given in the respective *yellow-red* and *cyan-blue scales*, respectively. The *black line* marks the pre-defined CoM path, while the two *grey lines* are the side boundaries of the sliding surface. The MNS lengthens significantly while sliding downslope, thus becoming much thinner. Part of it remains on land, whereas its front reaches a depth of 550 m b.s.l
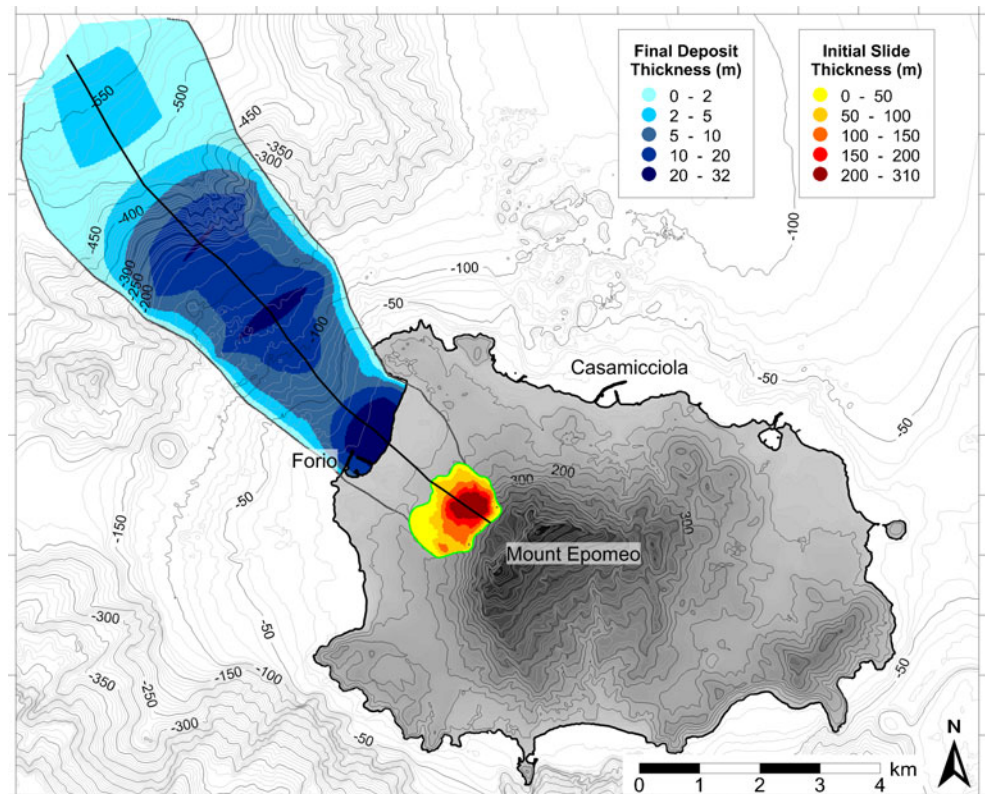


path common to all the centres of mass (CoM) of the slide blocks (hereafter referred to as the CoM path) and the lateral boundaries of the sliding surface (Fig. 2). The CoM path, the most likely trajectory for the sliding mass, follows the local slope gradient, from an elevation in excess of 400 m a.s.l to almost 600 m b.s.l. off the north-western coast. The lateral boundaries account for the transverse spreading of the mass during motion and are necessary to compute the transverse cross-sections of the moving blocks, whose size and shape affect the resistance forces in our slide computation. Furthermore, they influence the area affected by the slide and hence the source area of the tsunami.
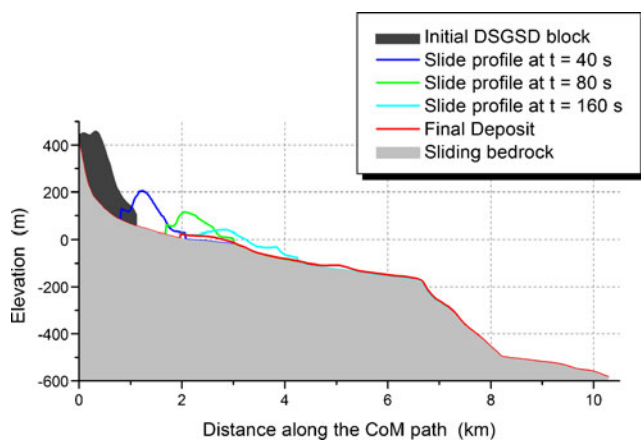
Cross-sections constructed along the CoM path at different times (Fig. 3) can throw further light on the evolution of the geometry of the sliding mass. The initial mobilized mass was subaerial, with the toe at about 100 m a.s.l. and the surface of rupture was a smooth concave prolongation of the island topography from the slide toe to the slide head (Fig. 3).

Simulation of MNS motion has been done using a 1-s time step for the input of the wider tsunami computational grid, G1, and 0.2 s for grid G2, which is smaller and focussed on Ischia (see paragraph on "Tsunami simulation"). The different time steps come from numerical stability requirements for the tsunami modelling, i.e. the distance travelled by the wave in a time-step must be smaller than the grid cell size. The basal friction coefficient values for the subaerial motion and the submarine part (see Appendix A), have been selected

according to the results of simulations of analogous events, in which they were tested against observational data of run-out distances (see Tinti et al. 2008, 2011). A bulk density of 2,000 kg/m$^3$ has been assigned to the sliding material, according to the lithological characteristics of the outcropping rocks.

The sliding mass shows a certain compactness in the initial subaerial phase, whereas when interacting with the sea it lengthens by more than 5 km and its average thickness value is accordingly reduced to 10–20 m. A portion of the mass (around $30 \cdot 10^6$ m$^3$; 20 % of the total) stops its descent across the coastline, with thickness exceeding 30 m at 0–10 m sea depth, causing a significant variation in coastal morphology. Notably, the harbour of Forio, one of the most important on the island, would be completely swept away about 60 s after slide initiation. The largest portion of the mass stops on the sub-horizontal submerged platform, between 100 and 150 m b.s.l. (Fig. 3), spreading consistently when entering the water. A small fraction of the mass (around 1 million m$^3$) overtops the north-western escarpment and reaches a depth of more than 500 m b.s.l., with a thickness of less than 10 m. The results of our simulation suggest that the flat offshore is very likely the main deposition area for masses coming from the north-western flank of Mt. Epomeo, as already recognized for past mass-wasting events (de Alteriis et al. 2010).

The simulated slide reaches its maximum block-average speed (almost 30 m/s) after about 30 s (Fig. 4a), following an

**Fig. 3** Cross-sections constructed along the CoM path (*black line* in Fig. 2) of MNS. Slide profiles at different times are plotted *above the top* of the topo-bathymetric section (in *grey*): the final deposit is depicted by the *red line* and the initial body is in *black*. Notice the substantial longitudinal spreading of the mass when moving undersea

initial phase of strong acceleration, due to the steep slopes of the initial portion of the sliding surface. This maximum velocity is in the same order of magnitude as the one (50–70 m/s) calculated for the larger Mount St. Helens rockslide-debris avalanche (Glicken 1998). The velocity curves of the individual blocks (Fig. 4a) are quite similar even after reaching the peak speed, highlighting that the slide initially moves as an almost coherent body. Indeed the blocks begin to travel with different velocities only when they reach the sea, as in our computation the bottom friction coefficient offshore is much smaller than the one on land. Consequently, when a block reaches the sea, it is affected by lower bottom resistance (here prevailing on the drag resistance) and starts moving faster than the blocks behind that are still on land (see the abrupt gradient change in the velocity curves between 60 and 100 s in Fig. 4a). Further accelerations and decelerations of the individual blocks between 100 and 500 s are due to block collisions and slight changes in the bathymetry gradient, for example close to the shoreline. At the end of the simulation, after 500 s, the front blocks overtop the escarpment and again accelerate downslope. Differential block velocities, with frontal blocks traveling faster than the others and the rear block stopping onshore before reaching the sea, cause the slide to lengthen and grow thinner.

Figure 4b shows the average and the individual values of the Froude number, which are defined as the ratio of the horizontal velocity of moving objects (here the entire slide or the single block) over the phase velocity of the tsunami, here computed as $\sqrt{gh}$, with $h$ local sea depth and $g$ gravitational acceleration. By definition the Froude number $Fr$ can be calculated only in the sea and measures the ability of the slide to transfer energy to the water waves. When it is close to 1, the resonance condition is attained, since slide and tsunami travel with the same speed and the energy transfer is

maximised. $Fr$ values departing from the critical value are indicative of lower tsunamigenic efficiency. When entering the sea with a finite speed, a block has a very high $Fr$ since the sea depth tends to zero, but $Fr$ values rapidly evolve from supercritical to subcritical values stabilizing on average around $Fr=0.4$. The simulation is stopped when the mass reaches the end of the computational domain, in this case after about 570 s. The mass is still in motion with most blocks travelling at 5 m/s or less, but it has lost almost all of its tsunamigenic capability since the corresponding $Fr$ values are low. Therefore, neglecting the further slide motion has negligible effect on tsunami computations.

Tsunami simulation

The UBO-TSUFD simulation code computes tsunami propagation over a single or a number of nested grids, made up of regularly spaced nodes at a given elevation. Since onshore and offshore databases are usually collected and organised independently, some irregularities and artefacts could result from merging them, especially in the near-shore zone that is exactly the area most critical for computing tsunami inundation and impact. Therefore, in tsunami studies, special attention has to be devoted to building meshes with the most accurate representation of the coastline. We have therefore used two distinct square-cell grids with different resolution. The grid G1, characterized by 200 m step, includes the coast of the Campanian Plain and the Gulf of Naples, while the grid G2, with 40 m cells, includes Ischia and the neighbouring island of Procida (Fig. 5).

After 3 min (Fig. 5a), the tsunami propagates with a strong positive leading front, spreading almost radially from the source zone. Two minutes later (Fig. 5b), this front, together with the following negative trough, has affected the entire western coast of Ischia, as well as the western portion of the northern coast, along which are the towns of Lacco Ameno and Casamicciola. The wave front also begins to deform, slowing down in the shallower sea north of the island while travelling faster in the south. After 10 min (Fig. 5c), the simulation shows many interesting features: (a) the tsunami has already circumnavigated the whole island; (b) a sequence of lows and highs are evident along the coast of the island, interpretable as trapped waves with seaward amplitude damping; (c) the island of Procida is attacked from the north-west by a strong 2-m amplitude positive wave, while a lower positive front approaches from the south-west; and (d) while some energy is scattered in the open sea, towards the north-west, a strong crest-trough sequence approaches the coast of the Campanian Plain with almost normal incidence. This front reaches the Campanian coast up to Castel Volturno (Fig. 5d, e, f) with a positive 2–3 m front, between 15 and 20 min after initiation. In the south the tsunami is weaker, affecting the island of Capri with waves less than 2 m high,
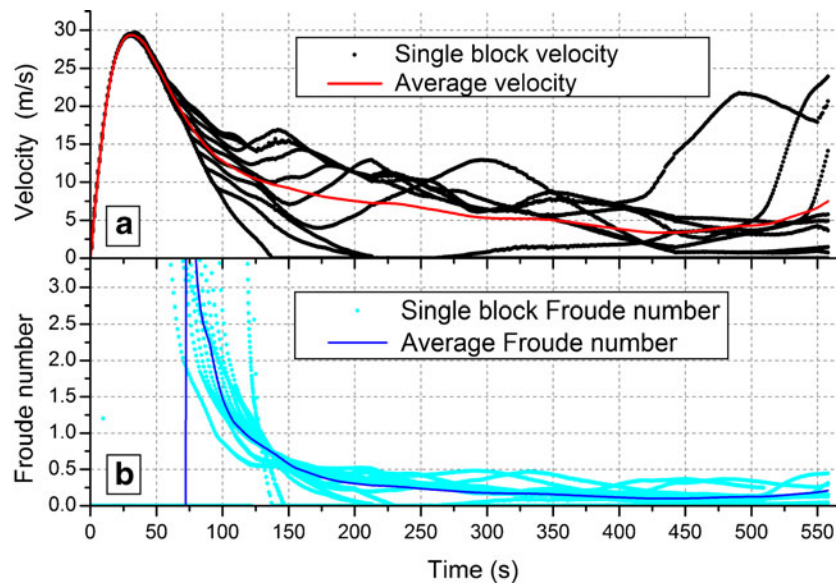
**Fig. 4** Velocity (*upper panel*) and Froude number (*lower panel*) vs. time. Velocity curves of single blocks (*black dotted*) and block average (*solid red line*) show that all blocks are synchronised while the slide moves on land, but have quite different speeds when it reaches the sea after about 60 s. The Froude number curves (*cyan dots* for single blocks and *red* for the slide) pass across the line of critical regime (*Fr* = 1) when blocks move near shore, just after entering the sea. The final simulation phase shows some blocks still moving at a high velocity, but the low Froude number of the individual blocks and of the whole slide indicate that the tsunamigenic potential is much lower and comparatively negligible

and the Gulf of Naples, especially the Sorrento Peninsula at its south-eastern border, with waves around 1 m high. The simulation also shows that, due to the particular morphology of the basin, tsunami energy is trapped for a long time in the
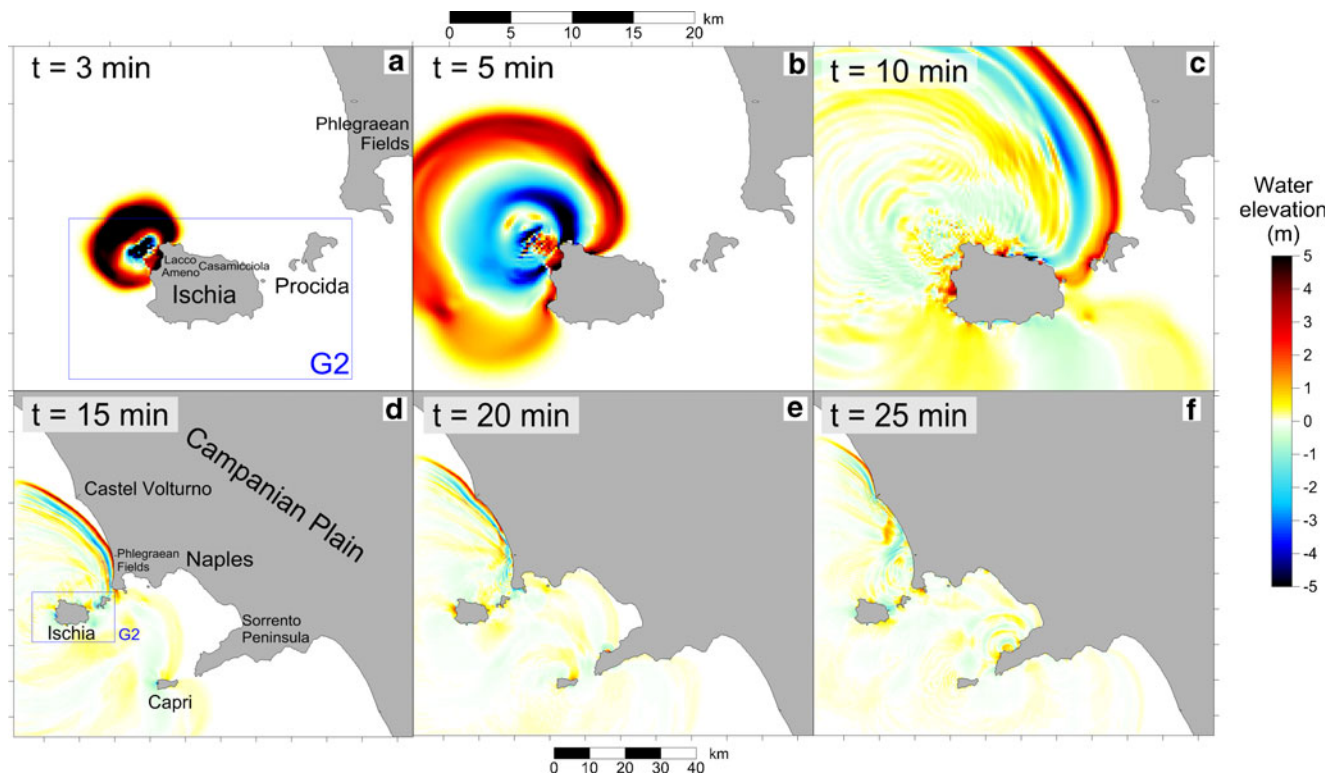


**Fig. 5** Tsunami propagation over grid G1 (zoomed in the first three sketches). The finer grid, G2, is delineated in *blue*. The positive waves, meaning water uplift and sea inundation at the coast, are marked in *yellow-red*, while the negative ones, corresponding to sea drop and retreat at the shore, in *cyan-blue*

**Fig. 6** Maximum sea surface elevation fields in grid G2, including the islands of Ischia and Procida. The *green dashed line* marks the side boundaries of the sliding surface
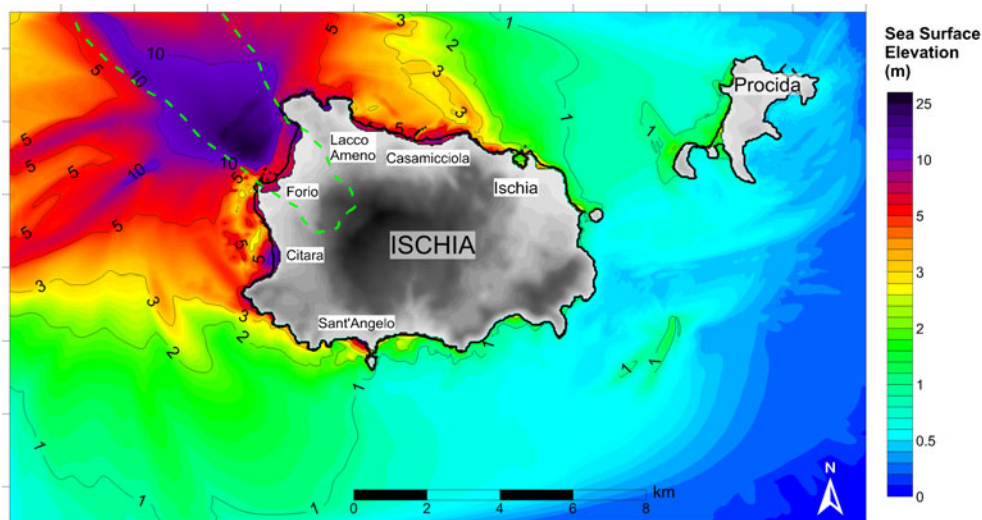


Gulf of Naples. This is not surprising since tsunamis are known to enhance local seiches and to persist in coastal basins like bays, gulfs, inlets, harbours, etc. (Roeber et al. 2010).

Tsunami propagation around the coasts of Ischia and Procida may be better appreciated by considering the higher-resolution grid G2 (Fig. 6). The highest values of the maximum water elevation computed in each node G2, as expected, occur along the path of the slide, since the slide front advancing on the sea floor has the main effect of pushing the water up and creating a leading crest (Fig. 5b). The largest part of the tsunami energy is channelled north-westward, but significant energy also heads towards the coast of Ischia. Along the northern coast, the maximum sea surface elevations exceed 8–10 m, rapidly decreasing eastward, while along the western shore, in the area of Citara, south of Forio, water waves are even higher, exceeding 10 m. The remaining coasts of Ischia and of the western side of Procida are impacted by 1–2 m high waves that have the potential to damage seaside infrastructure.

Synthetic marigrams (Fig. 7) can help complete the tsunami picture. In Lacco Ameno the tide gauge is on a node with a sea depth of 18 m. A first positive 4-m signal, arriving 4 min after the slide initiation, is followed by an equivalent sea level drop in about 4 min, and by other two relevant sea level oscillations. In general the tsunami seems to affect the

**Fig. 7** Synthetic marigrams computed in four virtual tide gauges located around Ischia and towards Procida (see their position in the *upper inlet*)
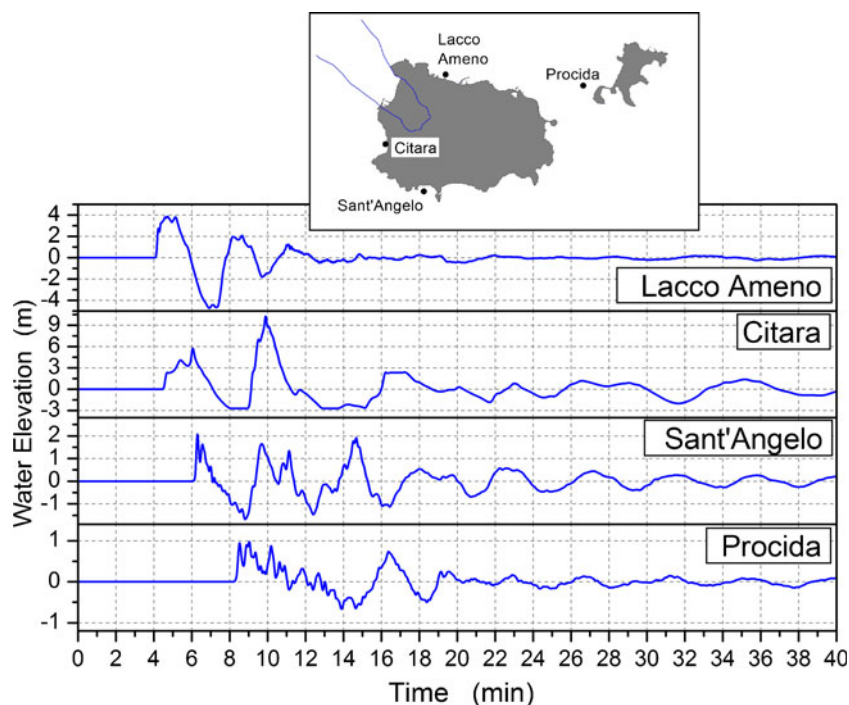
**Fig. 8** Maximum sea surface elevation in grid G1, covering the northern Campanian coast and Gulf of Naples coasts
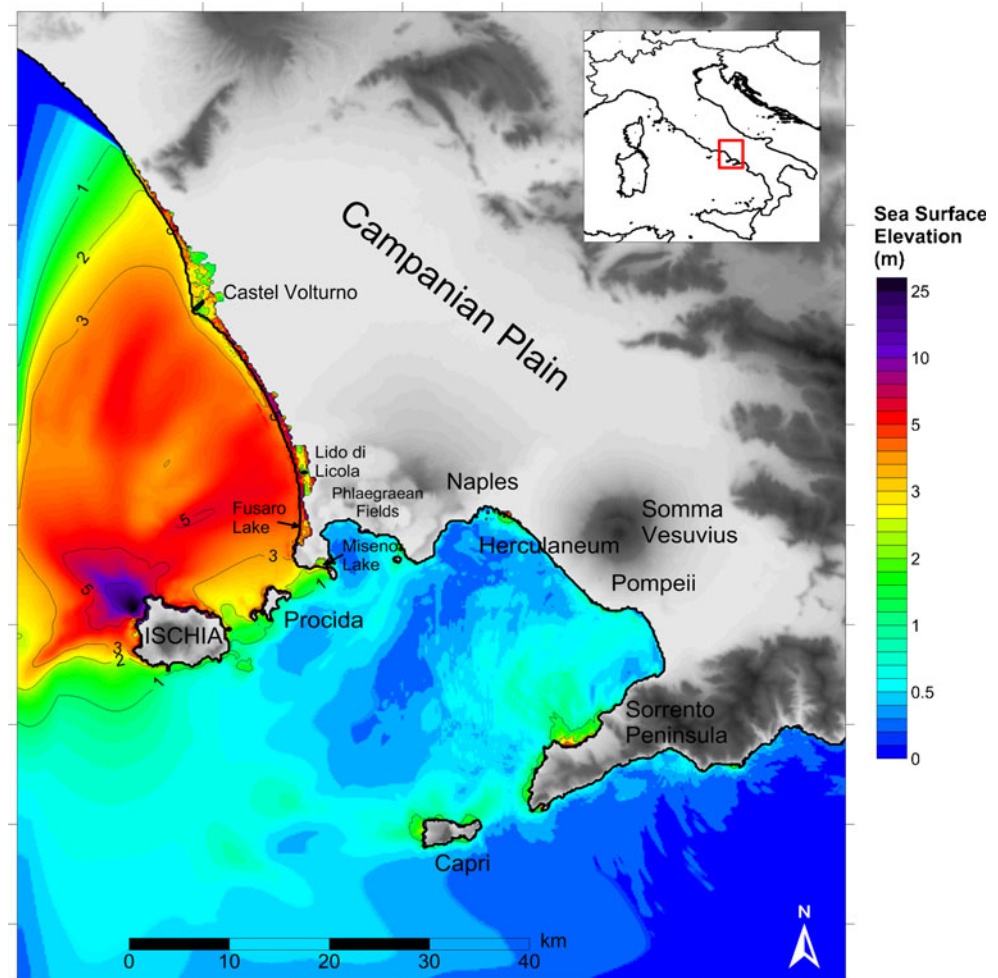
northern coast for more than 20 min. The sea-level time history in Citara shows even larger oscillations, with a first wave reaching 6 m amplitude, a complete sea withdrawal (the oscillation is cut at −3 m, since this is the sea depth in the node where the record is computed) and a subsequent maximum of more than 9 m. The perturbation, characterised by a dominant period of about 6 min, still produces waves of more than 1 m after 40 min. Along the southern coast, more protected from the arrival of destructive waves, the Sant'Angelo tide gauge (10 m sea depth) records a signal of more than 3 m peak-to-peak, that starts 6 min after the slide onset as a sea rise with a 4-min period. The fourth tide gauge, located towards the north-east, 2 km off Ischia (sea depth around 20 m), exhibits a 1 m wave starting about 8 min after the beginning of the landslide motion. This front moves towards Procida and its amplitude increases when approaching the coast where non-linear effects become important.

The propagation pattern of the MSN tsunami on the wider domain of the grid G1 (Fig. 8) is very interesting. The tsunami energy directs initially north-westward of the source region, but most of it is redirected north-eastward, namely towards the northern Campanian coast. Here it penetrates more than 2 km

inland around the very flat mouth of the Volturno river, and floods all the coastal area to the south to a width of several hundreds of meters. A small fraction of the tsunami energy also travels towards the south-east, hitting the island of Capri 40 km from source and the Sorrento Peninsula 20 km farther away, with the largest waves reaching 2 m, before entering the Gulf of Naples where it generates a mild wave perturbation.

## Assessment of tsunami effects in both near and far field

The MNS would have direct effects over the area impacted by the rock sliding and indirect effects resulting from the excited tsunami in the near-source region (i.e. along the Ischia coast) as well as in the mainland (Fig. 5). The slide would devastate an area of about 3.5 km², mostly within the town of Forio and to a lesser extent of Lacco Ameno (Fig. 6). In particular, about one fourth of the Forio territory, including the harbour and the existing infrastructures, would be destroyed. A preliminary estimate suggests that about 3,000 buildings might be swept away by the sliding mass. Furthermore, if unanticipated, the rock sliding would be lethal for many of the 18,000

**Fig. 9** Maximum water elevations on grid G2, with zooms over northern (*panel b*) and western (*panel c*) coasts. In *panel a*, the area affected by the landslide, i.e. within the sliding surface boundaries (*green dashed line*), is given. The inundated areas are visible as prolongation of the sea (*colour field*) onland. The buildings between 0 and 400 m a.s.l. are marked as *dots* (*grey-black in panels b* and *c*), permitting counting of those potentially flooded as well as those located along the trajectory of the sliding mass and swept by the sliding motion (*dark green dots in panel a*)
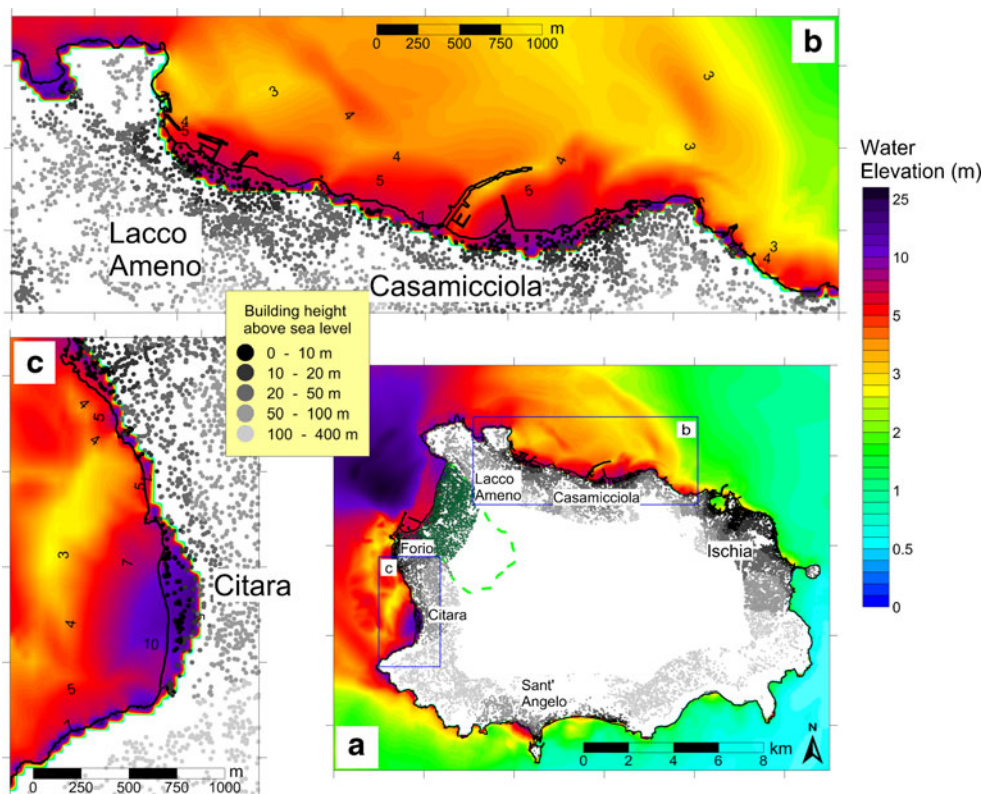
inhabitants of Forio. The induced tsunami would mostly affect the western and north-western coast of Ischia (Figs 6 and 9a) and the area between Castel Volturno and the Phlegraean Fields (Fig. 8). The tsunami would reach the western portion of the northern coast of Ischia with waves up to 10 m high. Since the coast is mostly high, the sea would penetrate inland only for 100–200 m in the towns of Lacco Ameno and Casamicciola, affecting some hundreds of buildings around the respective harbours (Fig. 9b). To the south of the landslide, the sea would inundate popular beaches and reach an altitude of 15 m in the area of Citara (Fig. 9c), involving some tens of structures, including hotels and thermal parks with spa facilities.

Outside Ischia, the area that would be mostly affected by the tsunami is characterised by low coasts and located towards the north, around the mouth of the Volturno river (Fig. 8). The flooded area would cover about 20 km² and belong mostly to Castel Volturno and in part to Mondragone towns. The tsunami would hit beaches and almost the entire urban territory of Castel Volturno, inhabited by more than 20,000 people, to a distance of 1–2 km from the shoreline, in addition to the marinas along the Volturno banks. The entire coast from Castel Volturno to the Phlegraean Fields, featuring some marinas and long flat tourist beaches, would be affected by the tsunami wave, with wider penetration in the areas of Lido di Licola and Fusaro lake. To the south, in the Miseno area, the flat land separating Miseno lake from the sea would be

flooded. In the Gulf of Naples the tsunami would be weaker and some inundation only would occur in the city of Naples.

## Conclusions

Our investigation of a hypothetical failure of Monte Nuovo DSGSD block and sliding of the mobilized mass into the sea, have yielded some interesting results in terms of generation and dynamics of both rock slide and tsunami, as well as of their effects on the territory, in particular in a densely inhabited area.

The MNS has a potential volume of about 0.16 km³ and covers an initial area of about 1.5 km². In our simulation, the sliding mass, moving as a compact body, attains a high velocity (about 30 m/s, after 30 s). The largest part of this mass enters the sea in the area of Forio after 60 to 120 s, while only about 20 % stops at the present shoreline and modifies the coast, producing 20–30 m thick deposits. The portion of the mass that reaches the sea continues its descent along the subhorizontal platform offshore of western Ischia, and its front runs down the continental scarp up to 500 m b.s.l., 5 km from the coastline.

Both rockslide-debris avalanche and the resulting tsunami generate damage on Ischia and along the adjacent continental coast. The slide devastates almost one fourth of the territory of the town of Forio. The tsunami affects the northern and

western coast of Ischia. Around the two small harbours of Lacco Ameno and Casamicciola almost all the buildings below 10 m a.s.l. are affected. The area of Citara, south of Forio, including popular beach and spa resorts, is severely hit by waves up to 15 m high, involving tens of buildings. As much as 20 km$^2$ of low land is inundated in the towns of Mondragone and Castel Volturno, with involvement of at least 20,000 people.

Although the waves are much higher and more powerful at Ischia than farther away, the tsunami produces more extensive flooding and causes greater damages along the Campanian coast than at Ischia, where the coast is generally too steep to permit sea penetration. A catastrophic picture thus arises from our simulation of Monte Nuovo failure.

This study should be considered a preliminary evaluation of the MNS hazard and invites more accurate investigations, including sensitivity analyses (e.g. testing different slide hypotheses), using finer resolution both for the landslide and for the tsunami computations, and eventually assessing vulnerability of buildings, structures and infrastructure in the flooded zones as well as potential damage and life loss. This is material however for on-going and future work.

The obtained results also permit one general consideration on tsunami propagation: its main features (Figs 6 and 8) depend mostly on the bathymetry, but also on the position and characteristics of the MNS source. Comparison of the MNS tsunami propagation scenario with that of the IDA (Tinti et al. 2011), supposedly involving the southern sector of Mt. Epomeo with a much larger debris mass and a much longer run-out distance, highlights that the tsunami near-field propagation scenarios around the island of Ischia are quite different: in this region the influence of the source is dominant over the tsunami propagation. Despite source and other differences, the two events have common features worth highlighting: (a) energy trapping in the Gulf of Naples and (b) refraction of the tsunami front leading to strong wave impact along the Campanian coast between the Phlegraean Fields and Castel Volturno. As these tsunami features are mainly determined by the bathymetry rather than by the source, we may conclude that they are common features to any tsunami scenario induced by landslides detaching from the Ischia slopes. In particular, we suggest that the flat coast north of the Phlegraean Fields up to the mouth of the Volturno river is highly vulnerable to the threat of tsunamis from landslides on Ischia.

## Appendix A. Analytical procedures

Landslide modelling

The landslide modelling applies a Lagrangian approach to a set of blocks that are obtained by discretizing the sliding body. This partition, in which blocks can change shape but not volume, well accounts for mass deformation during down-slope motion, a factor characterising the slide dynamics and influencing the consequent tsunami generation. The dynamic equations are solved by computing for each time step $i$, and for the centre of mass (CoM) of each block $k$, the value of the acceleration $a_{i,k}$ which is the sum of three terms (Eq. 1)

$$a_{i,k} = G_{i,k} + R_{i,k} + F_{i,k} \qquad (1)$$

$G_{i,k}$ accounts for the body forces (gravity, buoyancy) and for the basal friction between the block and the sliding surface. $R_{i,k}$ describes the drag forces due to the interaction between the exposed block surface and the environmental fluid (implying that it vanishes when the block moves subaerially). $F_{i,k}$ is the internal block-block interaction term, accounting for the reciprocal pushes between two contiguous blocks. This interaction, which is modelled like a particle collision and depends on the difference between the CoM velocities, tends to reduce the speed differences among the blocks with a corresponding loss of mechanical energy. A more detailed description of the procedure is given by Tinti et al. (1997). The simulation is stopped when the sliding mass exits the computational domain or when its block-averaged velocity falls below a pre-defined threshold.

The procedure has been implemented in two versions: in the 1D version (UBO-BLOCK1) the mass is split into a "train" of blocks, and the forces acting on the mass are projected along a pre-defined path, that is shared by all the CoMs. The transversal size of the slide is reconstructed by means of a predefined shape function and plays a subordinate role in the computation of the slide motion. It influences the acceleration through the resistance term $R_{i,k}$ that also depends on the lateral size of the exposed block surface. For this reason the code can be considered 1.5D. In the 2D approach that is implemented in the code UBO-BLOCK2, the mass is partitioned into a mesh of blocks that can interact not only along the direction of the motion but also laterally. It has been found that for a landslide in which length dominates over width, and therefore lateral variations are less important, the code UBO-BLOCK1 is adequate to compute its evolution.

Tsunami modelling

The propagation of the tsunami is computed by solving the non-linear non-dispersive Navier–Stokes equations in the shallow water approximation given by the following set of Eq. (2)

$$\partial_t \eta = \partial_t h_s - \nabla \cdot [(h + \eta)\mathbf{v}]$$
$$\partial_t \mathbf{v} = -g\nabla \eta - (\mathbf{v} \cdot \nabla \mathbf{v}) \qquad (2)$$

that express respectively mass and momentum conservation; $\eta$ is the water elevation with respect to the undisturbed still level, $h$ the local sea depth, v is the horizontal depth-averaged velocity and $g$ the gravitational acceleration. The term $h_s$ is the variable representing the local thickness of the sliding mass, that at a given location increases when the slide arrives and returns to zero when the slide passes completely across the point, acting as a "forcing term" exciting the tsunami. It is computed by the landslide code and then adapted in the tsunami simulation by means of the interpolation code called UBO-TSUIMP. This latter code, in addition to a geometrical grid-to-grid mapping, also applies a filter depending on the local water depth: the deeper the water in which the slide moves, the lower the tsunamigenic signal reaching the sea surface.

The code UBO-TSUFD solves the equations given in (Eq. 2) through a finite-difference numerical scheme (leap-frog staggered-grid method), over a regular rectangular-cell grid, covering the computational domain and representing bathymetry and topography. The spatial resolution can be changed, zooming over a region of particular interest, by nesting two or more grids of different cell size within one another.

As for the boundary conditions, a pure transmission condition is applied on the open-sea boundaries, while a moving boundary algorithm is implemented on the coasts allowing the computation of run-up heights and inland inundation. For further details on the tsunami codes refer to Tonini et al. (2011). The landslide and tsunami simulation codes briefly described above have been extensively applied by some of the authors to investigate historical and pre-historical tsunamigenic mass failures, such as those that occurred at the island of Vulcano in 1988 (Tinti et al. 1999), and at Stromboli in 2002 (Tinti et al. 2006). Further examples can be found in Tinti et al. (2000), (2003), (2011); Argnani et al. (2011) and Lo Iacono et al. (2012).

## References

Abadie SM, Harris JC, Grilli ST, Fabre R (2012) Numerical modeling of tsunami waves generated by the flank collapse of the Cumbre Vieja Volcano (La Palma, Canary Islands): Tsunami source and near field effects, J Geophys Res - Oceans 117, C05030. doi:10.1029/2011JC007646

Acocella V, Funiciello R (1999) The interaction between regional and local tectonics during resurgent doming: the case of the island of Ischia, Italy. J Volcanol Geoth Res 88:109–123. doi:10.1016/S0377-0273(98)00109-7

Acocella V, Funiciello R, Marotta E, Orsi G, de Vita S (2004) The role of extensional structures on experimental calderas and resurgence. J Volcanol Geoth Res 129:199–217

Agliardi F, Crosta G, Zanchi A (2001) Structural constraints on deepseated slope deformation kinematics. Eng Geol 59:83–102. doi:10.1016/S0013-7952(00)00066-1

Argnani A, Tinti S, Zaniboni F, Pagnoni G, Armigliato A, Panetta D, Tonini R (2011) The eastern slope of the southern Adriatic basin: a case study of submarine landslide characterization and tsunamigenic potential assessment. Mar Geophys Res 32:299–311. doi:10.1007/s11001-011-9131-3

Brown RJ, Orsi G, de Vita S (2008) New insights into Late Pleistocene explosive volcanic activity and caldera formation on Ischia (southern Italy). B Volcanol 70(5):583–603. doi:10.1007/s00445-007-0155-0

Bruno PP, de Alteriis G, Florio G (2002) The western undersea section of the Ischia volcanic complex (Italy, Tyrrhenian Sea) inferred by marine geophysical data. Geophys Res Lett 29(9):1029–1034

Buchner G (1986) Eruzioni vulcaniche e fenomeni vulcanotettonici di età preistorica e storica nell'isola d'Ischia. In: Centre Jean Bérard, Institut Français de Naples (ed) Tremblements de terre, eruptions volcaniques et vie des hommes dans la Campanie antique, 7, pp 145–188

Chiesa S, Civetta L, De Lucia M, Orsi G, Poli S (1987) Volcanological evolution of the island of Ischia. Rend Acc Sci Fis Mat Napoli Special Issue, pp 69–83

Chiesa S, Civetta L, Orsi G, Poli S (1988) The recent volcanic history of Ischia. Soc Geol It, Atti 74 Cong Naz v B, pp 108–111

Chiocci FL, de Alteriis G (2006) The Ischia debris avalanche: first clear submarine evidence in the Mediterranean of a volcanic island pre-historical collapse. Terra Nova 18:202–209. doi:10.1111/j.1365-3121.2006.00680.x

Chiocci FL, Romagnoli C, Tommasi P, Bosman A (2008) The Stromboli 2002 tsunamigenic submarine slide: Characteristics and possible failure mechanisms. J Geophys Res 113, B10102. doi:10.1029/2007JB005172

Chiodini G, Avino R, Brombach T, Caliro S, Cardellini C, de Vita S, Frondini F, Marotta E, Ventura G (2004) Fumarolic and diffuse soil degassing west of Mount Epomeo, Ischia (Italy). J Volcanol Geoth Res 133:291–309

Choi BH, Pelinovsky E, Kim KO, Lee JS (2003) Simulation of the trans-oceanic tsunami propagation due to the 1883 Krakatau volcanic eruption. Nat Hazards Earth Sys 3:321–332

Ciotoli G, Della Seta M, Del Monte M, Fredi P, Lombardi S, Lupia Palmieri E, Pugliese F (2003) Morphological and geochemical evidence of neotectonics in the volcanic area of Monti Vulsini (Latium, Italy). Quatern Int 101–102:103–113

Civetta L, Gallo G, Orsi G (1991) Sr- and Nd-isotope and traceelement constraints on the chemical evolution of the magmatic system of Ischia (Italy) in the last 55 ka. J Volcanol Geoth Res 46:213–230

Civetta L, De Vivo A, Orsi G, Polara G (1999) Il vulcanismo ad Ischiain età Greco-romana secondo le evidenze geologiche e le testimonianze storico-letterarie. Vichiana, Rass Studi Filolog Stor IV(I):14–32

D'Argenio B, Aiello G, de Alteriis G, Milia A, Sacchi M, Tonielli R, Budillon F, Chiocci FL, Conforti A, De Lauro M, d'Isanto C, Esposito E, Ferraro L, Insinga D, Iorio M, Marsella E, Molisso F, Morra V, Passaro S, Pelosi N, Porfido S, Raspini A, Ruggieri S, Terranova C, Vilardo G, Violante C (2004) Digital elevation model of the Naples Bay and adjacent areas, eastern Tyrrhenian Sea. Atlas Italian Geologic Mapping, 32 IGC, Firenze, August 2004

de Alteriis G, Tonielli R, Passaro S, De Lauro M (2005) Batimetria dei fondali marini della Campania (Isole Flegree—Ischia e Procida). CNR—Consiglio Nazionale delle Ricerche, Istituto per l'Ambiente Marino Costiero (IAMC), Liguori Eds., Napoli

de Alteriis G, Violante C (2009) Catastrophic landslides off Ischia volcanic island (Italy) during prehistory, vol 322. The Geological Society, London, pp 73–104, Special Publications

de Alteriis G, Insinga D, Morabito S, Morra F, Chiocci FL, Terrasi F, Lubritto C, Di Benedetto C, Pazzanese M (2010) Age of submarine debris avalanches and tephrostratigraphy offshore Ischia Island, Tyrrhenian Sea, Italy. Mar Geol 278:1–18. doi:10.1016/j.margeo.2010.08.004

de Vita S, Sansivero F, Orsi G, Marotta E (2006) Cyclical slope instability and volcanism related to volcano-tectonism in resurgent calderas:

the Ischia island (Italy) case study. Eng Geol 86:148–165. doi:10.1016/j.enggeo.2006.02.013

de Vita S, Sansivero F, Orsi G, Marotta E, Piochi M (2010) Volcanological and structural evolution of the island of Ischia (Italy) over the past 10 ka. In: Groppelli G, Viereck-Goette L (eds) Stratigraphy and geology of volcanic areas. Geological Society of America, Special Paper 464: 193–241. doi: 10.1130/2010.2464(10)

Del Prete S, Mele R (2006) Il contributo delle informazioni storiche per la valutazione della propensione al dissesto nell'Isola d'Ischia. Rend Soc Geol It, Nuova Serie 2:29–47

Della Seta M, Del Monte M, Fredi P, Lupia Palmieri E, Sbarra P (2005) Fractal analysis and morphological evolution of volcanic relief: some examples from Italy. Z Geomorphol Supp 140:1–18

Della Seta M, Marotta E, Orsi G, De Vita S, Sansivero F, Fredi P (2011) Slope instability induced by volcano-tectonics as an additional source of hazard in active volcanic areas: the case of Ischia island (Italy). B Volcanol 74:79–106. doi:10.1007/s00445-011-0501-0

Di Napoli R, Aiuppa A, Bellomo S, Brusca L, D'Alessandro W, Gagliano Candela E, Longo M, Pecoraino G, Valenza M (2009) A model for Ischia hydrothermal system: evidences from the chemistry of thermal groundwaters. J Volcanol Geoth Res 186(3–4):133–159. doi:10.1016/j.jvolgeores.2009.06.005

Di Napoli R, Martorana R, Orsi G, Aiuppa A, Camarda M, De Gregorio S, Gagliano Candela E, Luzio D, Messina N, Pecoraino G, Bitetto M, De Vita S, Valenza M (2011) The structure of a hydrothermal system from an integrated geochemical, geophysical, and geological approach: The Ischia Island case study. Geochem Geophy Geosy 12 (7), Q07017. doi:10.1029/2010GC003476

Francis PW (1985) The origin of the 1883 Krakatau tsunamis. J Volcanol Geoth Res 25:349–369

Glicken H (1998) Rockslide-debris avalanche of May 18, 1980, Mount St Helens volcano, Washington. B Geol Soc Jpn 49:55–106

Lo Iacono C, Gràcia E, Zaniboni F, Pagnoni G, Tinti S, Bartolomé R, Masson D, Wynn R, Lourenço N, Pinto de Abreu M, Dañobeitia JJ, Zitellini N (2012) Large and deep slope failures in the Gorringe Bank: Evidence for landslide-generated tsunamis along the SW Iberian Margin. Geology 40:931–934. doi:10.1130/G33446.1

Manzo M, Ricciardi GP, Casu F, Ventura G, Zeni G, Borgstrom S, Berardino P, Del Gaudio C, Lanari R (2006) Surface deformation analysis in the Ischia Island (Italy) based on spaceborne radar interferometry. J Volcanol Geoth Res 151:399–416

McCoy FW, Heiken G (2000) Tsunami Generated by the Late Bronze Age Eruption of Thera (Santorini), Greece. Pure Appl Geophys 157: 1227–1256

NGDC/WDS—National Geophysical Data Center/World Data System, Global Historical Tsunami Database, Boulder, CO, USA. (Available at http://www.ngdc.noaa.gov/hazard/tsu_db.shtml)

Nomanbhoy N, Satake K (1995) Generation Mechanism of Tsunamis from the 1883 Krakatau Eruption. Geophys Res Lett 22(4):509–512. doi:10.1029/94GL03219

Orsi G, de Vita S, Di Vito M, Isaia R, Nave R, Heiken G (2003) Facing volcanic and related hazards in the Neapolitan area. In: Heiken G, Fakundiny R, Sutter J (eds) Earth Sciences in the City. American Geophysical Union (Special Publication), Washington, pp 121–170

Orsi G, Gallo G, Zanchi A (1991) Simple shearing block-resurgence in caldera depressions. A model from Pantelleria and Ischia. J Volcanol Geoth Res 47:1–11

Orsi G, Patella D, Piochi M, Tramacere A (1999) Magnetic modeling of the Phlegrean Volcanic District with extension to the Ponza archipelago, Italy. J Volcanol Geoth Res 91:345–360

Orsi G, Piochi M, Campajola L, D'Onofrio A, Gialanella L, Terrasi F (1996) 14C geochronological constraints for the volcanic history of the island of Ischia (Italy) over the last 5,000 years. J Volcanol Geoth Res 71:249–257

Pareschi MT, Favalli M, Boschi E (2006) Impact of the Minoan tsunami of Santorini: Simulated scenarios in the eastern Mediterranean, Geophys Res Lett 33, L18607. doi:10.1029/2006GL027205

Pelinovsky E, Zahibo N, Dunkley P, Edmonds M, Herd R, Talipova T, Kozelkov A, Nikolkina I (2004) Tsunami Generated by the Volcano Eruption on July 12–13, 2003 at Montserrat, Lesser Antilles. Sci Tsunami Hazards 22(1):44–57

Radbruch-Hall D, Varnes DJ, Colton RB (1977) Gravitational spreading of steep-sided ridges ("sackung") in Colorado. J Res US Geol Surv 5:359–363

Roeber V, Yamazaki Y, Cheung KF (2010) Resonance and impact of the 2009 Samoa tsunami around Tutuila, American Samoa, Geophys Res Lett 37, L21604. doi:10.1029/2010GL044419

Satake K (2007) Volcanic origin of the 1741 Oshima-Oshima tsunami in the Japan Sea. Earth Planets Space 59:381–390

Satake K, Kato Y (2001) The 1741 Oshima-Oshima Eruption: Extent and Volume of Submarine Debris Avalanche. Geophys Res Lett 28:427–430

Sepe V, Ventura G, Vilardo G (2009) Integrated methodologies for 3d deformation analysis at Ischia island (Italy): state of the art, prospectives and modelling. In CD "Final Programme and Proceedings" of the 6° International Symposium on Digital Earth, 9–12 September, Beijing, China, 042960275.pdf, 1–6

Ter Stepanian G (1966) Type of depth creep of slopes in rock masses. Problems Geomech 3:49–69

Tinti S, Bortolucci E, Armigliato A (1999) Numerical simulation of the landslide-induced tsunami of 1988 on Vulcano Island, Italy. B Volcanol 61:121–137

Tinti S, Bortolucci E, Romagnoli C (2000) Computer simulations of tsunamis due to flank collapse at Stromboli, Italy. J Volcanol Geoth Res 96:103–128

Tinti S, Bortolucci E, Vannini C (1997) A block-based theoretical model suited to gravitational sliding. Nat Hazards 16:1–28

Tinti S, Chiocci FL, Zaniboni F, Pagnoni G, de Alteriis G (2011) Numerical simulation of the tsunami generated by a past catastrophic landslide on the volcanic island of Ischia, Italy. Mar Geophys Res 32(1):287–297. doi:10.1007/s11001-010-9109-6

Tinti S, Pagnoni G, Zaniboni F (2006) The landslides and tsunamis of the 30th of December 2002 in Stromboli analysed through numerical simulations. B Volcanol 68:462–479. doi: 10.1007/s00445-005-0022-9

Tinti S, Pagnoni G, Zaniboni F, Bortolucci E (2003) Tsunami generation in Stromboli and impact on the south-east Tyrrhenian coasts. Nat Hazards Earth Sys 3:299–309

Tinti S, Zaniboni F, Pagnoni G, Manucci A (2008) Stromboli Island (Italy): scenarios of tsunamis generated by submarine landslides. Pure Appl Geophys 165:2143–2167. doi:10.1007/s00024-008-0420-y

Tonini R, Armigliato A, Pagnoni G, Zaniboni F, Tinti S (2011) Tsunami hazard for the city of Catania, eastern Sicily, Italy, assessed by means of Worst-case Credible Tsunami Scenario Analysis (WCTSA). Nat Hazards Earth Sys 11:1217–1232. doi:10.5194/nhess-11-1217-2011

Varnes DJ, Radbruch-Hall D, Savage WZ (1988) Topographic and structural conditions in area of gravitational spreading of ridges in the western United States, vol 1496. US Geological Survey Paper, Washington, pp 1–2

Vezzoli L (1988) Island of Ischia. In: Vezzoli L (ed) CNR Quaderni de"La ricerca scientifica", 114–10, 122 pp

Ward SN, Day S (2001) Cumbre Vieja Volcano - Potential collapse and tsunami at La Palma, Canary Islands. Geophys Res Lett 28(17): 3397–3400. doi:10.1029/2001GL013110

Ward SN, Day S (2003) Ritter Island Volcano - lateral collapse and the tsunami of 1888. Geophys J Int 154:891–902. doi:10.1046/j.1365-246X.2003.02016.x